Check for updates

Advances in the green and controllable synthesis of MWW zeolite

Yanan Wang,[a] Yu Zhang,[ab] Weifeng Chu,[a] Yang Gao,[a] Sujuan Xie,*[a] Xiujie Li, [ID] [a] Longya Xu [ID] *[a] and Xiangxue Zhu [ID] [a]

MWW zeolite is one of the commercialized zeolites that shows great promise in heterogeneous catalysis and other interdisciplinary application fields due to its coexisting multi-channel system. The green and controllable synthesis of MWW zeolite is conducive to its more efficient and broader application. Many researchers focus on precisely controlling the dimension, interlayer hydroxyl condensation, and aluminum siting, as well as obtaining MWW with low-toxicity, readily available organic structure directing agents (OSDAs) or without OSDAs. This review summarizes recent advancements in the synthesis and application of MWW zeolite, with a particular emphasis on selecting different OSDAs, controlling the interlayer condensation degree and adjusting aluminum distribution. Future research directions and development trends of MWW zeolite are also forecasted.

1 Introduction

MWW zeolite, a microporous zeolite, is among the commercially available zeolites out of the approximately 260 recognized zeolite structures. While only about 20 of these structures have been successfully commercialized, MWW zeolite stands out due to its remarkable performance in various petrochemical processes. MWW zeolite is a promising material in heterogeneous catalysis, especially in alkylation, isomerization, catalytic cracking, disproportionation, adsorption, and so on.[1] Besides, metal/metal oxide-MWW zeolite bifunctional catalysis also shows adjustable catalytic performance in oxidation, reduction, and many other reactions due to its unique multi-channel system.

The layer MWW zeolite features two independent pore systems. One is the intralayer 10 member ring (MR) sinusoidal channels and the other is interlayer 12 MR supercages. Additionally, there are some hemi-supercages (pockets) distributed on the surface (Fig. 1).[2] This unique channel system and multiple interlayer condensation degrees contribute to a diverse MWW zeolite family with various order degrees and interlayer distances. These variations result in differences in active site distribution and catalytic performance. The MWW family comprises several members, including MCM-22, MCM-49, ITQ-1, ITQ-2, SSZ-25, EBR-1, MCM-56, MCM-36, PSH-3, Ti-MWW and so on.

Since the synthesis of MWW zeolite in the 1990s, the highly toxic hexamethyleneimine (HMI) has commonly been used as an organic structure directing agent (OSDA), leading to challenges in developing low toxic or OSDA-free methods for synthesizing MWW zeolite. Despite efforts to find alternative OSDAs, the process remains complex and OSDA-free synthesis of MWW zeolite is still in its early stages. Furthermore, achieving precise control over its dimension and interlayer hydroxyl condensation remains challenging when using a single, low-toxicity, readily available template. Another obstacle is the exposure of more pocket-active sites of MWW zeolite while maintaining good thermal stability. This article provides a comprehensive overview of the synthesis and application of MWW zeolite, including a detailed examination of OSDAs for MWW zeolite and methods for regulating interlayer condensation and Al distribution. The future research and development tendency of MWW zeolite is also discussed.

2 Synthesis of MWW zeolite

MWW zeolite is usually hydrothermally synthesized with the assistance of OSDA. The expensive and highly toxic hexamethyleneimine (HMI) is one of the most commonly used OSDAs for the synthesis of MWW zeolite with diverse properties, which shows superiority to other OSDAs. Researchers have been committed to looking for lower toxicity OSDAs or OSDA-free synthetic strategies in the early stages. With the development of research, it has been found that the layer thickness and Al siting of MWW zeolites play a critical role in controlling their acidity and catalytic performance. Numerous methods have

[a] *State Key Laboratory of Catalysis, Dalian Institute of Chemical Physics, Chinese Academy of Sciences, Dalian 116023, Liaoning, China. E-mail: sjxie@dicp.ac.cn, lyxu@dicp.ac.cn*

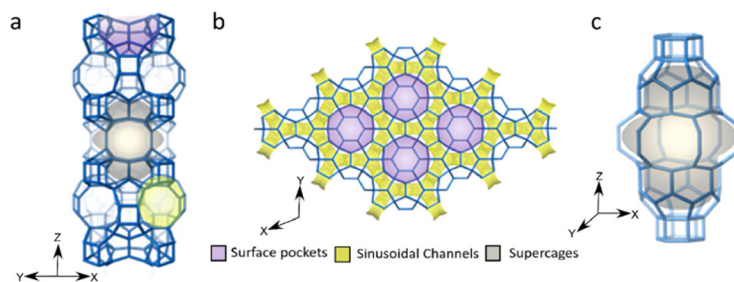[b] *University of Chinese Academy of Science, Beijing 100049, China*

Fig. 1 The topology of MWW zeolite from ref. 2. Copyright 2022 American Chemical Society. (a) 12-MR pockets on the external surface (purple), 10-MR windows accessing internal supercages (gray), and 10-MR sinusoidal channels (yellow). (b) Top-down view along the [001] direction. (c) Supercage.

been developed to synthesize MWW zeolite with unique properties precisely.

2.1 OSDAs for the synthesis of MWW zeolite

HMI is usually employed as the OSDA to hydrothermally synthesize silica–alumina MWW zeolite. HMI is superior to other OSDAs, because it can obtain products in a wide range of synthesis composition with diverse physicochemical properties. Unfortunately, HMI is costly and highly toxic, which goes against the goals of green synthesis. Therefore, researchers have focused on seeking (1) a second OSDA (cyclohexylamine (CHA) and piperazine *etc.*), which can reduce the HMI content; (2) a lower toxicity OSDA, such as CHA, piperidine (PI), 1-admantammonium, and so on; and (3) an OSDA-free method.

Wu *et al.*[3] prepared MCM-22 zeolite with HMI and a piperazine binary template agent. When piperazine content accounted for 78% of the total template agent content, pure MCM-22 zeolite was still successfully synthesized, although piperazine was often used as the OSDA to synthesize ZSM-5. In our previous work,[4] HMI and CHA binary amines were used as the OSDA to synthesize MCM-22 and the usage of HMI can be reduced. In the HMI-CHA binary amine template system, HMI only played a structure-directing role and CHA stabilized the framework of the MCM-22 by filling the pores. CHA is a typical OSDA for FER zeolite that easily produces intergrowth with MWW zeolite,[5–7] making it challenging to synthesize pure MWW only with CHA.

In our recent work, MCM-49 zeolite was firstly synthesized using CHA as an OSDA by suppressing the growth of FER zeolite at low temperatures,[8] and it was found that CHA is mainly distributed in supercages and semi-supercages. For a long time, with PI as the OSDA, only MCM-22 zeolite and boron-containing EBR-1 zeolite can be obtained.[9] Recently, MCM-49 zeolite has also been obtained using PI as the OSDA by a comprehensive balance of organic template and inorganic ions.[10] The synthesis composition range of MCM-22 and MCM-49 zeolite is divided in the PI system. The obtained samples exhibited comparable catalytic performance with MCM-49 zeolite using HMI as the OSDA in the liquid alkylation of benzene with ethylene.

Besides, other alternative OSDAs have been reported. MWW zeolites with different morphologies like ellipsoid, wool ball, and uniform hexagon were synthesized by changing the Na salts species when using 1-butyl-2,3-dimethyl-1*H*-imidazol-3-ium hydroxide as the OSDA.[11] The use of diethyldimethyl ammonium hydroxide could be used to synthesize UZM-8 zeolite with a structure similar to MCM-56.[12,13] Wu *et al.*'s research team first prepared interlayer split ECNU-5A and ECNU-5B zeolite using 1,3-bis(cyclohexyl)imidazolium hydroxide as a template.[14] Subsequently, a new three-dimensional MWW zeolite ECNU-10 was synthesized using 1-amantadine as the template.[15] Recently, some new template agents have been proposed to synthesize MWW zeolite. Grzybek *et al.*[16] synthesized UJM-1P zeolite with a layer spacing of 2.6 nm by interlayer modification from monolayer MWW zeolite using biquaternary ammonium salt as a template agent. The interzeolite conversion method has also been used to synthesize MWW zeolite, which has the advantage of shortening the crystallization time, reducing the crystalline size, and regulating the acid distribution, but the OSDA is indispensable.[17–19]

Pure silica MWW (ITQ-1) zeolite can only be synthesized in HMI and *N,N,N*-trimethylmonoglyl ammonium hydroxide (TMAdaOH) double template system at the earliest,[20] and can be synthesized in the TMAdaOH single template system later, but the crystalization time is long (more than 5 days) and the repeatability is poor.[21,22] Lu *et al.*,[23] for the first time, synthesized pure silicon MWW zeolites with long chain cations of imidazolium in a fluorine-containing system and found that the template agent mainly existed in sinusoidal channels and surface semi-supercages in the layer, and fluorine ions existed in $[4^6 6^4]$ and $[4^1 5^2 6^2]$ cages. Hong *et al.* successfully synthesized high-silicon MCM-22 zeolite using *N,N,N,N,N*-pentamethyl-1,5-pentanediaminium as the template.[24] By introducing the boron, the SAR of the product in the HMI system can be widened to 30–600.[25]

To sum up, compared to the OSDAs that are complex or not readily available, CHA and PI can be regarded as "green" OSDAs (Fig. 2).

Undoubtedly, the real green method to obtain zeolites is free of OSDAs, which can reduce the cost and avoid the formation of harmful gases and polluted water. Kamimura[26] firstly reported the OSDA-free synthesis of 2D MCM-22 zeolite using a seed directing method. However, it is still challenging to precisely synthesize MWW zeolite with specific properties *via* the OSDA-free method (Fig. 3(a)). In our work, the highly crystallized MCM-49 zeolite was obtained using the as-made MCM-49
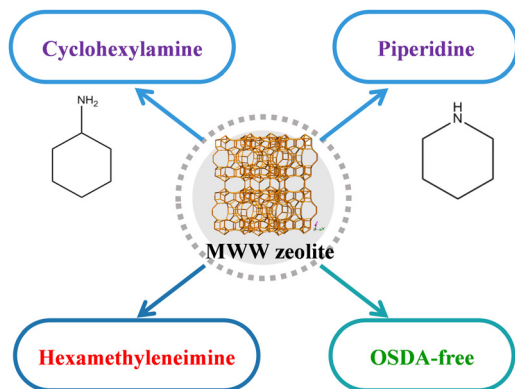
Fig. 2 Synthesis of MWW zeolite with low toxicity OSDA or OSDA-free methods in our recent work.

zeolite as the seed without the addition of OSDA under mild conditions (140 °C, 30–38 h) with the aid of the ultrasonic aging procedure[27] (Fig. 3(b)). With ultrasonic aging, MCM-49 seed integrity was retained and also both the silica and aluminium species were promoted to move to the solid phase, which was conducive to the growth of MCM-49 zeolite in the absence of OSDA.

2.2 MWW family with various interlayer condensation degrees

The multiple interlayer condensation degree of the MWW zeolite contributes to a diverse MWW zeolite family. This leads to a discrepancy in active site distribution and catalytic performance,[28–34] as well as the catalytic performance of metal-MWW catalyst.[35,36] By controlling the interlayer condensation, the thickness of the layer can be adjusted to synthesize different kinds of MWW zeolite, such as 2D MCM-22(P), 3D MCM-49, delaminated MCM-56, pillaring MCM-36, monolayer ITQ-2, and so on.

The delaminated MWW structure has a large external surface, more exposed active sites, and rich silanol groups, leading to remarkable catalytic performance. In order to reduce the layer thickness of the MWW zeolite, post-synthesis (top-down) and direct synthesis (bottom-up) methods have been developed.

2.2.1 Post-synthesis method. The transformation between 2D and 3D structures is a unique characteristic of the layer zeolite, which can be realized by post-treatment (Fig. 4(a)). MCM-22(P) layer precursor produces 3D MCM-22 zeolite frameworks upon calcination, or similar treatment to remove the interlayer OSDAs, inducing layer condensation. Besides, the layer precursor can be exfoliated to delaminated/single layer MCM-56/ITQ-2 zeolite upon acid treatment or silylated/pillared to IEZ-MWW/MCM-36.[37] However, the post-exfoliation method often needs harsh conditions to preserve the structure, resulting in the loss of solid yield.

Besides, silanols of opposed layers can be condensed by nitric acid treatment, and the template extraction and shrinkage of the interlayer distance can be adjusted by controlling the acid concentration.[40] In Silva et al.'s work,[41] the delamination of MCM-22 zeolite can be realized by the ball mill method, rather than chemical surfactants and sonication, which has comparable or improved physical properties compared to chemically delaminated MCM-22 zeolite without a significant loss of acid sites.

2.2.2 Direct synthesis method. For a long time, various MWW family zeolites could only be synthesized in the typical HMI system. Kennedy et al.[42] found that the final product phase was dependent on the molar ratio of silica to alumina (SAR) in the HMI system, and the SARs of MCM-22(P) and MCM-49 zeolite ranged from 21 to 31 and 17 to 22, respectively. It was also revealed that the product phase was related with the synthesis gel composition, especially the molar ratio of OSDA to Na species.

Efforts to directly synthesize exfoliation zeolites have been made and it is usually necessary to introduce additional templates or additives. MWW layers with a thickness of 3.5 nm can be generated using the exfoliating agent cetyltrimethylammonium (CTA$^+$) to avoid post-synthesis exfoliation[38] (Fig. 4(b)). Xu et al. proposed an approach to hydrothermally synthesize delaminated Al-SSZ-70 zeolite with CTA$^+$ and diisobutylimidazolium.[43] MWW zeolite with two layers was synthesized by Wang et al. with dual templates as OSDAs[39] (Fig. 4(c)). A direct epitaxial synthesis of 2D MWW zeolite, with an average thickness of 10 nm and an aspect ratio of over 50, is guided by HMI and hexagonal boron nitride, which can
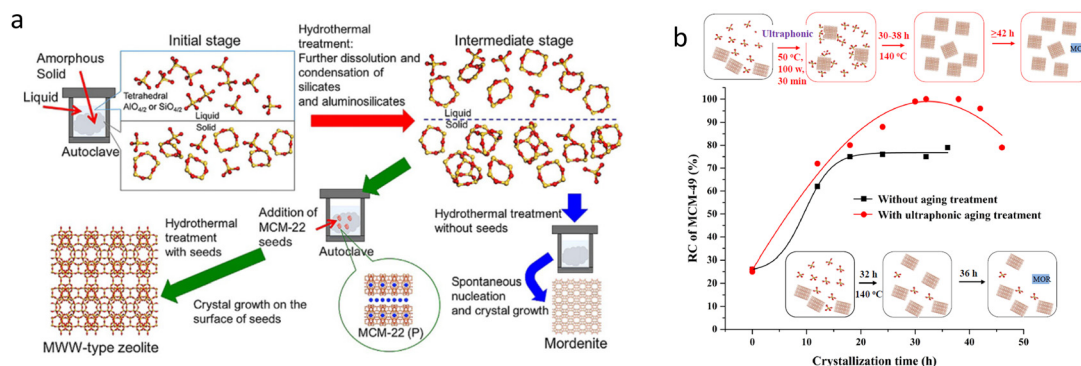

Fig. 3 OSDA-free synthesis of MWW zeolite from ref. 26 (a) Copyright 2017 Wiley-VCH and ref. 27 (b) Copyright 2021 Royal Society of Chemistry.
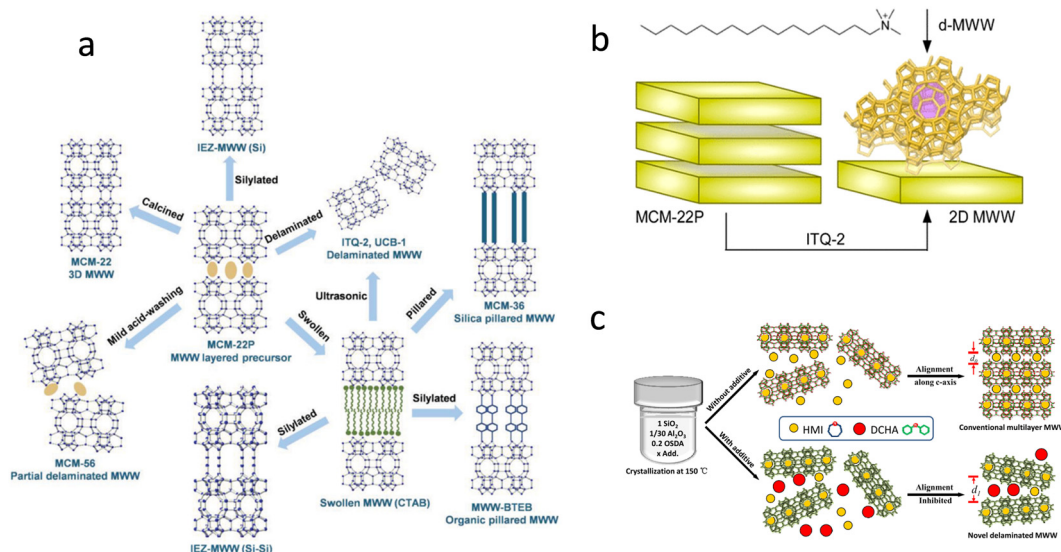
Fig. 4 Description of the post-synthetic modifications of 2D layered zeolite precursors from ref. 37 (a) Copyright 2016 Wiley–VCH and direct synthesis of exfoliation zeolites from ref. 38 (b) Copyright 2020 American Chemical Society and ref. 39. (c) Copyright 2020 Elsevier B.V.

increase the product selectivity and shed light on more efficient catalysis and precise molecule separation.[44] Single to multiple-layer MWW zeolites were synthesized in Chen *et al.*'s work with HMI and amphiphilic organosilan.[45]

MCM-56 zeolite, as a typical delaminated MWW zeolite, is usually obtained by breaking the interlayer connection of MCM-22 precursor with acid treatment. Then Roth found that MCM-56 zeolite was an intermediate during the crystallization of MCM-49. If the crystallization process was intercepted before or around the time it started to turn into MCM-49 zeolite, the product was MCM-56.[46,47] OSDAs of large size can suppress interlayer condensation. EMM-10P with a misaligned MWW structure was obtained with bis(*N,N,N*-trimethyl)-1,5-pentanediaminium dibromide as an OSDA.[48] The layers of EMM-10P are disordered but still hydrogen bonded through interlayer silanols. ITQ-30 zeolite, with disordered layers as MCM-56 zeolite, was obtained using a very large and rigid molecular of *N*(16)-methyl-parthenium as OSDA.[49] By introducing a crystal growth modifier, the interlayer Si–O–Al bridge formation can be hindered, and delaminated MCM-56 zeolite with good stability can be obtained. Thinner-layered MCM-49 zeolite (with crystal sheets size of ∼200 nm and thickness of 5–20 nm is synthesized in the HMI system by Jiang *et al.* by using diquaternary ammonium salts to prevent the condensation of interlayer Si–O–Al bridges).[50] Then, they synthesized MCM-56 zeolite using a green and nuisance-less choline chloride as the OSDA instead of the toxic HMI template with the assistance of ITQ-1 zeolite.[51] A thinner-layered MCM-49 zeolite with 5–20 nm of thickness was achieved by adding additional diquaternary ammonium salts with long alkyl chains.[52]

Precisely controlling the interlayer hydroxyl condensation has prominent scientific significance for the green and efficient synthesis of MWW zeolite. However, there is a lack of efficient methods to control the interlayer hydroxyl condensation degree in an alternative template system except for HMI. In our recent work,[10] the rational and precise hydrothermal synthesis of MCM-22(P) and MCM-49 zeolite using low toxic PI as the OSDA, has been realized by comprehensively coordinating the competition of the organic template and inorganic ions. Our group strives to synthesize delaminated MCM-56 zeolite with low toxic OSDA, which promises to be realized soon. These works have important scientific significance in controlling the interlayer condensation of layered zeolite and will promote the efficiency of the catalytic process.

2.3 Regulation of the Al distribution

Al siting in a certain framework T site makes a great influence on the acidic property. The catalytic performance of zeolite is significantly influenced by its acid property resulting from the isomorphous substitution of Al for Si in lattice sites.[53,54] MWW zeolite has eight inequivalent T sites and a multi-channel coexistence structure. Our previous work demonstrated that the alkylation of benzene and ethylene mainly reacted in the supercage and surface pocket of MWW zeolite, and the contribution of sinusoidal channels was little[55] (Fig. 5(a)). So, directing more Al species siting in the supercage and semi-supercage is conducive to improving the alkylation performance of benzene and ethylene. The contribution of the acid sites in different pore systems of MWW zeolite to the syngas conversion to gasoline over the ZnCrOx-HMCM-49 catalyst was identified by Ding *et al.*[56,57] (Fig. 5(b)). They found the formation of gasoline and light paraffin was attributed to the acid sites in the sinusoidal channels and the supercages, respectively. For toluene alkylation with methanol, Parmar *et al.*[2] found that the acid sites in sinusoidal channels and supercages of MCM-22 zeolite were conducive to the improvement of *p*-xylene yield and catalyst stability (Fig. 5(c)).
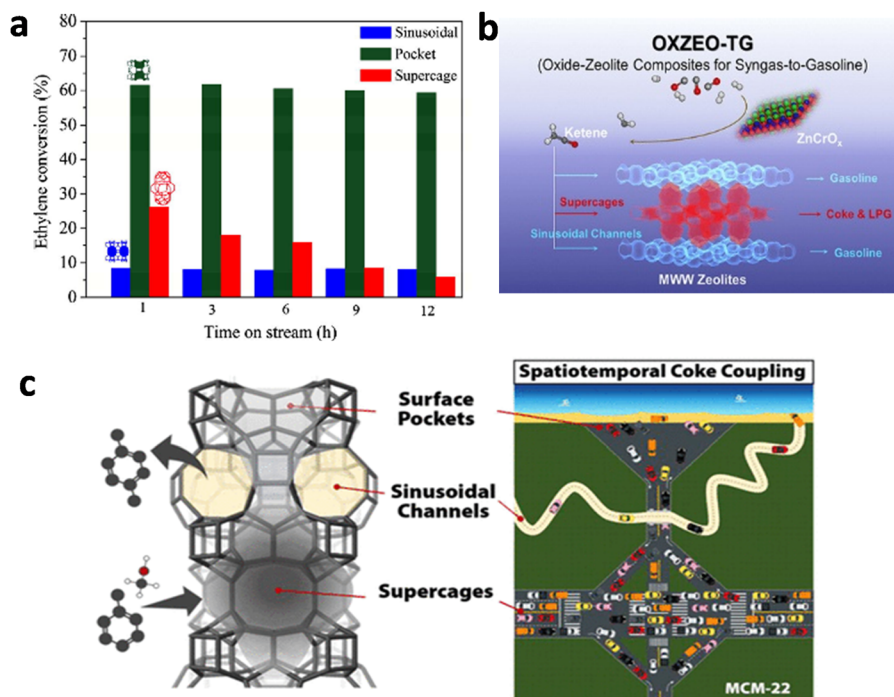
Fig. 5 (a) Catalytic role of different pore systems in MCM-49 zeolite for liquid alkylation of benzene with ethylene from ref. 58. Copyright 2011 Elsevier Inc. (b) The contribution of the acid sites in different pore systems of MWW zeolite to the syngas conversion to gasoline from ref. 59. Copyright 2023 American Chemical Society. (c) The contribution of sinusoidal channels and supercages of MCM-22 zeolite for toluene alkylation with methanol from ref. 2. Copyright 2022 American Chemical Society.

Many characterization methods have been developed to investigate the acid properties of zeolites. Temperature-programmed desorption of ammonia (NH_3-TPD) can test the acid concentration and acid strength. Pyridine adsorbed Fourier transform infrared spectroscopy (Py-IR) can provide the intensity and concentration of Brønsted acid sites and Lewis acid sites.[60] ^{1}H Magic-angle spinning nuclear magnetic resonance (MAS NMR) spectra and IR (hydroxyl region) can test the distribution of Brønsted acid sites, Lewis acid sites, and silanol. The Co^{2+} titration method combined with UV-visible spectroscopy has widely been adopted to indirectly analyze the number of paired and isolated Al atoms.[61] Solid-state ^{27}Al MAS NMR and 2D ^{27}Al MAS NMR can give a detailed information about the Al species located in a specific T site. Multinuclear and multidimensional correlation solid-state NMR techniques, including 2D ^{27}Al-^{1}H D-RINEPT with wPMRR recoupling and ^{1}H-^{27}Al D-HMQC MAS NMR experiments,[58] have been used to study the role of OSDAs in selective Al substitution. Besides, the theoretical methods have been employed to simulate the Al distribution and proton siting in the zeolite framework.[62]

Traditionally, the acid distribution is adjusted by introducing heteroatoms or removing aluminum through acid treatment. Wang et al.[59] impregnated MCM-22 zeolite with different amounts of phosphorus and found that the Brønsted acid sites were decreased by phosphorus modification. Tian et al.[63] used a similar method to prepare a phosphorous modified MCM-22 zeolite for the alkylation of benzene and 1-dodecene. They believed that the phosphorous modification had little influence on MCM-22 structure, but would change the acid strength due to the polymerized phosphate bond with Al. In Fan et al.'s work, the Brønsted acid sites in the sinusoidal channel of MCM-22 zeolite can be concentrated by appropriately inserting boron, which was conducive to improving the stability of methanol to olefin and the selectivity of propylene and butene.[64] They recently found that the deactivation behaviour of MTH over MWW zeolite was also related to the acid density and distribution.[65] The acid sites in supercages caused rapid deactivation, while the ones in sinusoidal channels were highly resistant to coke formation. Wang et al.[66] regulated the framework Al location of MCM-22 zeolite by the boron insertion method. The acid sites in the sinusoidal channels provided a good shape-selective space for the alkylation of benzene with methanol. Meanwhile, the decrease of Brønsted acid sites in the supercages and pockets enhanced the tolerance capacity to coke and catalytic life of MCM-22 zeolite. To reduce the Brønsted acid sites through dealuminization, Mihályi et al.[67] treated MCM-22 zeolite with hydrochloric acid and oxalic acid, thus improving the selectivity of m-xylene to p-xylene. Also, more Al species in the supercages can be exposed by selectively removing Si species in the supercages by alkali treatment with the assistance of CTAB, resulting in the improved catalytic performance of MCM-49 zeolite in anisole acylation with acetic anhydride.[68] Many other factors can affect the Al siting of MWW zeolite, such as OSDA species, inorganic cations, synthesis conditions, pore structures etc. Compared with the micron-sized MCM-22 zeolite synthesized by traditional methods, the
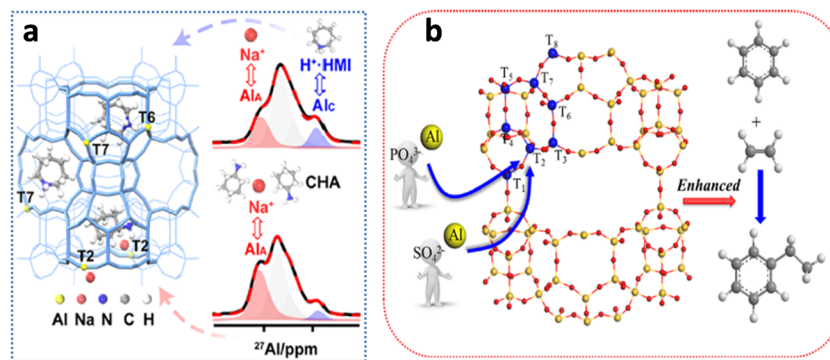
Fig. 6   Adjustment of the Al siting in MWW zeolite from ref. 71 (a) Copyright 2021 American Chemical Society and ref. 72 (b) Copyright 2018 Elsevier Inc.

nano-sized MCM-22 zeolite showed a decrease in Brønsted acid active sites and an increase in Lewis acid sites under a similar Si–Al ratio.[69]

In our work, it was found that synergism between HMI (or CHA) and inorganic metal ions exhibited a significant impact on the incorporation of framework Al. Compared with HMI, CHA led to more Al species of T_2 site, due to different protonation degrees of HMI and CHA. Most HMIs were in protonation state, while about half of CHAs were in a non-protonation state. The non-protonated CHA and Na^+ synergistically promoted the formation of MWW structure with preferential T_2 site of Al substitution[70] (Fig. 6(a)). In the synthesis system of MCM-22 zeolite with PI as OSDA, the Al siting was regulated by adding an additional anion in the synthesis gel. With addition of PO_4^{3-} or SO_4^{2-}, the resultant MCM-22 shows higher ethylene conversion than MCM-22 synthesized without additives in the alkylation of benzene with ethylene. It was attributed that more Al species were directed to T_2 site in the presence of PO_4^{3-} or SO_4^{2-} ref. 71 (Fig. 6(b)).

Besides, Al distribution has a close association with the degree of interlayer condensation. Suppressing the interlayer condensation can expose more Al siting in the surface pockets, while directing more Al species distributing on T_1 site can affect the interlayer condensation degree. For example, during the pillaring of MCM-22 to MCM-36 zeolite, the Brønsted acid sites were significantly reduced and the number of silicon hydroxyl groups was significantly increased.[72–75] ITQ-2 and MCM-56 zeolites showed higher acid content than MCM-22 zeolite due to their more active sites exposed in the delaminated structure. The MWW layer stacking mode can be changed when the intralayer T_1-OH pairs condensation is suppressed by leading more Al sited in T_1.[76] In a word, comprehensively balancing the Al siting and interlayer condensation is conducive to the rational and precise synthesis of MWW zeolite.

2.4   Preparation of hierarchical MWW zeolite

Hierarchical zeolites have an advantage in reducing the diffusion limitation, which is beneficial to the improvement of catalyst efficiency. Various attempts have been made to develop efficient methods to prepare hierarchical zeolites within the past decades.

Alkali treatment is a common method to construct mesopores in zeolites. After NaOH treatment, MCM-22 zeolite showed improved catalytic performance, which was attributed to the removal of the skeletal Si atoms, the formation of mesopores and the increase in the concentration of strong Brønsted and Lewis acid sites.[77] In our previous work, the template-containing MCM-22 zeolite was treated with NaOH, and the change in texture properties, element composition, and acid properties were studied.[78] Besides, hierarchical MCM-49 zeolite with intracrystalline mesopores was prepared by post-treating the MCM-49 zeolite in CTAB and NaOH mixed solution.[79] It was found that template content in the zeolite[80] and the alkali concentration[81] played an important role in preparing hierarchical MCM-49 zeolite.

Recently, a new method, H_2O_2-induced micro-explosion after ethanolamine treatment, was developed to synthesize hierarchical MWW nanosheets with c-axis penetrated mesopores.[82] Besides, hierarchical MCM-22 zeolites were synthesized in the presence of organosilane using HMI as the OSDA. The mesopores were produced by removing organosilane, accompanied by good preservation of the microporous nature of MCM-22.[83]

3   Application of MWW zeolite

The IZA organization has identified around 260 zeolite structures. However, only about 20 of them have been commercialized. MWW zeolite (MCM-22), patented in 1990, appears to be the last new framework developed for commercial use.[84] MWW zeolite shows excellent catalytic performance in many acid-catalyzed reactions, especially alkylation, due to its multi-channel system and adjustable acid properties (Fig. 7). However, the layer zeolite has disadvantages in thermal/hydrothermal stability, when used in high-temperature and water-presented reactions. Efforts towards suitable MWW zeolite synthesis methods should be made to balance the thermal/hydrothermal stability and the exposure degree of acid sites.

3.1   Application in alkylation of benzene and olefins

MWW zeolite shows excellent catalytic performance in the alkylation process of aromatics and low-carbon olefins. Taking
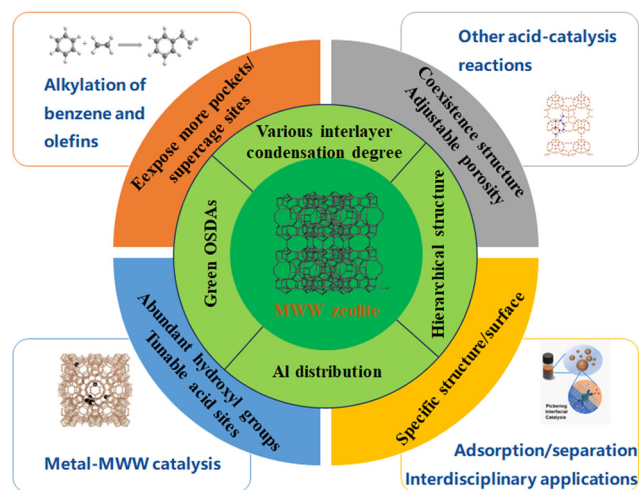
Fig. 7 Green and controllable synthesis of MWW zeolite and its application.

the reaction of benzene and ethylene as an example, compared with USY, ZSM-5, and beta molecular sieves, MWW zeolite has higher ethylbenzene selectivity because the 10-membered ring window can fully ensure the diffusion of raw materials, the supercage provides a place for reaction, and the 10-membered ring window prevents the diffusion of macromolecules such as diethylbenzene and triethylbenzene. Compared with beta zeolite, MWW zeolite has higher low temperature reactivity and can operate at low benzene/ethylene ratios, as does the alkylation of benzene with propylene.[85]

In the 1990s, MCM-22 catalyst was used in the production of ethylbenzene by Mobil. Subsequently, efforts were made to improve the activity. The ratio of feed benzene and energy consumption was significantly reduced, and the catalyst had good stability with a one-way running lifetime of more than three years.[86] Then, Lummus/UOP used a new MWW configuration of UM-8 with a high product yield in the alkylation of benzene with ethylene.[87] Recently, the double-layered MWW zeolite exhibited superior catalytic performance to conventional MCM-22 zeolite.[39]

Our research team recognized different contributions of surface pockets, supercages and sinusoidal channels of MWW zeolite to the alkylation reaction of benzene and ethylene[55] and deduced that the target reaction mainly reacted in the supercage and surface pocket of MWW. Additionally, due to the exposure of more active sites and reduced mass transfer resistance, the hierarchical MCM-22 zeolite showed higher ethylene conversion, ethylbenzene selectivity and reaction stability during the alkylation between benzene and ethylene.[79,88] Low toxicity and cheap CHA or PI were used as the OSDA to direct the crystallization of MWW zeolite and the obtained MWW product showed a similar alkylation performance compared with its counterpart using traditional HMI as an OSDA.[8,10,71] Also, the shaped MCM-49-CHA catalyst has shown excellent catalytic stability in a 1000 h lifetime test.[89]

Besides, MWW zeolite shows an outstanding alkylation performance of benzene and high-carbon olefins. Liang *et al.* studied the alkylation of benzene with 1-dodecene over MCM-36, MCM-22, and single layer MWW zeolite.[90] They found that MCM-36 zeolite had the highest apparent activation energy, revealing that the acid sites located on the external surface and within surface pockets of MWW zeolites were adequate for this reaction. Pillared MWW nanosheets with optimized Al distribution were excellent catalysts for the alkylation of benzene with 1-dodecene.[91] Cyclohexylbenzene, as a high-value-added organic intermediate, can be synthesized *via* the alkylation of benzene with cyclohexene or cyclohexanol. The delaminated MWW zeolite, with more accessible active sites than the 3D MWW zeolite, showed good catalytic performance in benzene alkylation with cyclohexene.[92]

3.2 Application in other acid-catalysis reactions

Due to the unique channel system of MWW zeolite, it shows special advantages in many acid-catalysis reactions compared to other zeolites. As well as the application in alkylation mentioned in Section 3.1, MWW zeolite can also be used in catalytic cracking,[25,93–95] isomerization,[96] disproportionation,[97–99] aromatization[100–102] and so on.[59] The supercages of MCM-22 are good places for many reactions. Matias *et al.* found that the acid sites in supercages of MCM-22 were responsible for 97% of *n*-heptane transformation (including main reactions of *n*-heptane isomerization, cracking, and aromatization), while the acid sites in sinusoidal channels made little contribution.[103]

MWW zeolite is an excellent catalyst for catalytic cracking.[94] In He's work, ZSM-5, beta, and MCM-22 were used as FCC catalysts, the gasoline and diesel yields of MCM-22 catalyst were higher than that of ZSM-5 and similar to that of beta, and MCM-22 showed a lower gas product yield than ZSM-5 and a higher one than beta.[95] In addition, they also found that MCM-22 had a high hydrogen transfer activity, and 12 MR supercages played an important role. MCM-22 zeolites with SAR of 30 to 600 were used in the catalytic cracking of 1-butene to propene. The increase of SAR could effectively suppress the formation of propane and aromatics, and the optimal selectivity to propene was obtained on the sample with a SAR of 158.[25]

MCM-22 also shows higher catalytic activity than ZSM-5 in the toluene disproportionation to *p*-xylene (PX) for its supercages.[98] MCM-22 introduced electron deficient InO^+ species, favoring preferential formation of PX due to an enhanced process of methyl transfer. In toluene disproportionation, the formation of PX mainly occurred within the supercages of MCM-22, while the isomerization of PX to *o*- and *m*-xylene was in the sinusoidal channels of MCM-22 at 473–573 K. The selectivity of PX in xylene isomers over MCM-22 was higher than its thermodynamic equilibrium value and further increased with the dealumination of MCM-22.[97] In Ren's work, the selectivity of PX was improved by silica deposition on the external surface of MCM-22.[99]

3.3 Application in bifunctional catalysis of metal–zeolite

The abundant hydroxyl groups and tunable Brønsted acid sites (BAS) of MWW zeolite are beneficial for introducing or anchoring metal active sites, which have significantly extended its applications in recent years such as ethane dehydrogenation,[104,105] conversion of alcohols to olefins,[106] dry reforming of methane,[107] oxidative hydration of ethylene,[108] carbohydrate conversion,[109–113] oxidation of volatile organic compounds,[114–116] and NH_3-SCR.[117]

Deborated ERB-1 or delaminated MWW zeolite (discussed in Section 2.2) have abundant defect sites, which are conducive to loading metal sites. The atom-planting introduced $GaCl_3$ into deborated MWW zeolite showed good dehydrogenation activity and stability in the direct dehydrogenation and CO_2 oxidative dehydrogenation of ethane.[118] A similar method could be used to introduce Sn into the zeolite framework and disperse on the external surface of the 'half-cup' supercage, which showed long-term alkane dehydrogenation conversion and stability.[119]

The encapsulation of metals in MWW zeolite can be realized by using the unique characteristics of transformation between 2D and 3D. Due to the abundant terminal silanols and defect sites of delaminated MWW, catalysts prepared by introducing metal to the swelling/delaminating MWW zeolite exhibit extraordinary catalytic performance in many reactions.[120–122] Single Pt atom and Pt clusters with exceptionally high thermal stability were generated by incorporating Pt during the transformation of a 2D MWW zeolite into 3D.[123,124] The Pt@MCM-22 showed strong thermal stability and shape selectivity in the dehydrogenation of propane to propylene. It is found that the single atom and smaller Pt clusters are encapsulated in semi-supercages, and the larger Pt clusters are encapsulated in supercages. The Ru clusters confined in zeolite and Brønsted acid sites were adjacent and had a synergistic effect, resulting in the improvement of catalytic activity and product selectivity.[125] Compared to the large metal particles, the sub-nanometric Ru clusters confined in MWW zeolite with a thickness of 20–30 nm show a significant improvement in hydrodeoxygenation activity. Singer-layer Ni/ITQ-2 catalysts exhibited higher carbon dioxide reforming of methane performance than the Ni/MCM-22 catalysts.[126] Recently, Zhang et al. reported that framework Fe atom of Fe-MWW could stabilize the single atom Pt confined into zeolite (Pt@Fe-MWW).[127] The Pt–O–Fe in Pt@Fe-MWW reduced the dissociation energy of the C–H bonds and facilitated the desorption of H_2, resulting in efficient dehydrogenation of propane.

3.4 Application in adsorption and separation

MWW zeolite has an open pore structure, narrow pore size distribution, high specific surface area, and high pore volume, which indicates that it holds potential for applications in adsorption and environmental purification.

Corma et al. investigated the diffusion properties of aromatic compounds over different zeolites and found that MCM-22 zeolite showed a lower diffusion coefficient than other zeolites because the residence time of molecules in big cavities with four entrance windows was higher than that in straight and sinusoidal channels.[128] The adsorption behaviors of methanol, methanal, toluene, ethylbenzene, and styrene molecules in FAU, FER, CON, and MWW zeolites were investigated in Zhao's work. The saturated adsorption capacity of the single component in various different zeolites decreased in the order FAU > MWW > CON > FER.[129]

MWW zeolite has the ability to adsorb both big aromatic compounds and small-molecule gases, due to its multi-channel coexistence structure and adjustable porosity.[130] In Pawlesa's work, they found that the highest CO_2 adsorption capacity was obtained on Na-MCM-49 with SAR of 30, and the lowest adsorption capacity was obtained over material containing the largest Cs^+ cation.[131] The adsorption capacity of MWW zeolite depends significantly on the nature and the concentration of the charge-compensating cations. Zukal et al. found that the CO_2 adsorption capacity of MWW zeolite in the low pressure region could be markedly increased due to the incorporation of magnesium oxide.[132]

Wang et al. investigated the adsorption capacity of MCM-22 zeolite for various dyes and found that it had the strongest adsorption capacity for methylene blue dye.[133,134] The adsorption kinetics followed the pseudo-second-order model and the external diffusion was the controlling process. In addition, they also found that MCM-22 had a good adsorption capacity for heavy metals and humic acids in wastewater.[135] Therefore, MCM-22 could have potential applications in wastewater treatment.

3.5 Application in interdisciplinary applications

In the latest progress on MWW zeolite, many interdisciplinary applications have emerged, due to its unique structure/surface properties.[84] Zeolite films, synthesized by alternate layer-by-layer growth of MWW zeolite with a stacking distance of 2–3 nm, are regarded as more favorable for high-precision and high-sensitivity sensors, ultrathin catalysts layers, adsorbents, and ion exchangers.[136] The exfoliation and surface functionalization of MCM22(P) can be used for multifunctional integrated protection of paper-based relics.[137] Zeng et al.[138] found that MWW could be used as a Pickering emulsion material to emulsify the organic-aqueous diphase system for its intrinsic amphiphilicity (readily abundant hydrophilic Si–OH group and lipophilic acid sites). There is potential for zeolite nanosheets in the exploitation of zeolite membranes and they could have promising potential applications in water purification.[139]

4 Conclusions

The exceptional catalytic performance of MWW zeolite in traditional alkylation processes and various petrochemical applications has been well-established. Surprisingly, MWW zeolite exhibits a wide range of interdisciplinary applications. The environmentally friendly and controllable synthesis of MWW zeolite is crucial for enhancing its efficiency and

expanding its utility. Although the highly toxic HMI retains an incomparable advantage over other OSDAs, the low toxicity and readily available CHA and PI exhibit tremendous potential in the controllable synthesis of MWW family zeolites with specific properties, positioning them as green OSDAs. Efforts toward achieving OSDA-free synthesis of MWW zeolite are ongoing. Besides, achieving a comprehensive balance between Al siting and interlayer condensation in MWW zeolite is conducive to the rational and precise synthesis and modification of its catalytic performance, as well as that of other zeolites.

Data availability

No primary research results, software or code have been included and no new data were generated or analysed as part of this review.

Conflicts of interest

There are no conflicts to declare.

Acknowledgements

References

1 P. Chatterjee, Y. Han, T. Kobayashi, K. K. Verma, M. Mais, R. K. Behera, T. H. Johnson, T. Prozorov, J. W. Evans, I. I. Slowing and W. Huang, *ACS Appl. Mater. Interfaces*, 2023, **15**, 54192–54201.
2 D. Parmar, S. H. Cha, T. Salavati-fard, A. Agarwal, H. Chiang, S. M. Washburn, J. C. Palmer, L. C. Grabow and J. D. Rimer, *J. Am. Chem. Soc.*, 2022, **144**, 7861–7870.
3 X. Wu, Y. Li, J. Jiang and S. Wei, *Chem. Eng.*, 2009, **4**, 18–19.
4 X. L. Niu, S. J. Xie, H. B. Li, T. Y. Jiang and L. Y. Xu, *Chin. J. Catal.*, 2005, **26**, 851–854.
5 W. Chu, X. Li, X. Zhu, S. Xie, C. Guo, S. Liu, F. Chen and L. Xu, *Microporous Mesoporous Mater.*, 2017, **240**, 189–196.
6 W. Chu, F. Chen, C. Guo, X. Li, X. Zhu, Y. Gao, S. Xie, S. Liu, N. Jiang and L. Xu, *Chin. J. Catal.*, 2017, **38**, 1880–1887.
7 Y. Wang, Y. Gao, W. Chu, D. Zhao, F. Chen, X. Zhu, X. Li, S. Liu, S. Xie and L. Xu, *J. Mater. Chem. A*, 2019, **7**, 7573–7580.
8 W. Chu, X. Li, S. Liu, X. Zhu and L. Xu, *J. Mater. Chem. A*, 2018, **6**, 12244–12249.
9 D. Nuntasri, P. Wu and T. Tatsumi, *J. Catal.*, 2003, **213**, 272–280.
10 Y. Wang, Z. Wang, S. Xie, W. Chu, X. Li, G. Hou and X. Zhu, *Chem. Eng. J.*, 2024, **487**, 150321.
11 W. Zi, Z. Hu, X. Jiang, J. Zhang, C. Guo, K. Qu, S. Tao, D. Tan and F. Liu, *Molecules*, 2024, **29**, 170.
12 S. H. Cha, L. Jin, J. Shin and S. B. Hong, *Top. Catal.*, 2015, **58**, 537–544.
13 Y. Shi, E. Xing, W. Xie, F. Zhang, X. Mu and X. Shu, *Ind. Eng. Chem. Res.*, 2019, **58**, 7725–7733.
14 L. Xu, X. Ji, J. G. Jiang, L. Han, S. Che and P. Wu, *Chem. Mater.*, 2015, **27**, 7852–7860.
15 P. Ji, M. Shen, K. Lu, B. Hu, J. G. Jiang, H. Xu and P. Wu, *Microporous Mesoporous Mater.*, 2017, **253**, 137–145.
16 J. Grzybek, W. J. Roth, B. Gil, A. Korzeniowska, M. Mazur, J. Cejka and R. E. Morris, *J. Mater. Chem. A*, 2019, **7**, 7701–7709.
17 P. Pornsetmetakul, F. J. A. G. Coumans, J. M. J. J. Heinrichs, H. Zhang, C. Wattanakit and E. J. M. Hensen, *Chem. – Eur. J.*, 2024, **30**, e202302931.
18 Y. Shi, E. Xing, E. Gao, D. Liu, W. Xie, F. Zhang, X. Mu and X. Shu, *Microporous Mesoporous Mater.*, 2014, **200**, 269–278.
19 E. Xing, Y. Shi, A. Zheng, J. Zhang, X. Gao, D. Liu, M. Xin, W. Xie, F. Zhang, X. Mu and X. Shu, *Ind. Eng. Chem. Res.*, 2015, **54**, 3123–3135.
20 M. A. Camblor, C. Corell, A. Corma, M.-J. Díaz-Cabañas, S. Nicolopoulos, J. M. González-Calbet and M. Vallet-Regí, *Chem. Mater.*, 1996, **8**, 2415–2417.
21 M. A. Camblor, A. Avelino Corma, M. Díazcabañas and C. Baerlocher, *J. Phys. Chem. B*, 1998, **102**, 44–51.
22 F. Rosso, A. Airi, M. Signorile, E. Dib, S. Bordiga, V. Crocellà, S. Mintova and F. Bonino, *Microporous Mesoporous Mater.*, 2024, **366**, 112924.
23 P. Lu, L. Gomez-Hortiguela and M. A. Camblor, *Chem. – Eur. J.*, 2019, **25**, 1561–1572.
24 L. Songho, S. Chaeho and S. B. Hong, *Chem. Lett.*, 2003, **32**, 542–543.
25 G. Xu, X. Zhu, X. Niu, S. Liu, S. Xie, X. Li and L. Xu, *Microporous Mesoporous Mater.*, 2009, **118**, 44–51.
26 Y. Kamimura, K. Itabashi, Y. Kon, A. Endo and T. Okubo, *Chem. – Asian J.*, 2017, **12**, 530–542.
27 Y. Wang, X. Li, Y. Gao, F. Chen, Z. Liu, J. An, S. Xie, L. Xu and X. Zhu, *Inorg. Chem. Front.*, 2021, **8**, 2575–2583.
28 Z. Zhang, J. Yang, J. Cui, Z. Li, C. Yang, Y. Ma and Q. Zhang, *ChemistrySelect*, 2023, **8**, e202204016.
29 D. S. D. Lima, L. L. Silva, I. W. Zapelini, S. Mintova and L. Martins, *Inorg. Chem. Front.*, 2023, **10**, 5649–5661.
30 G. Lee, E. Jang, T. Lee, Y. Jeong, H. Kim, S. Lee, Y. G. Chung, K.-S. Ha, H. Baik, H.-G. Jang, S. J. Cho and J. Choi, *Catal. Today*, 2023, **411–412**, 113856.
31 W.-H. Hu, M.-N. Liu, Q.-X. Luo, J. Zhang, H. Chen, L. Xu, M. Sun, X. Ma and Q.-Q. Hao, *Chem. Eng. J.*, 2023, **466**, 143098.
32 Y. Han, P. Chatterjee, S. B. Alam, T. Prozorov, I. I. Slowing and J. W. Evans, *Phys. Chem. Chem. Phys.*, 2023, **25**, 4680–4689.
33 R. Barakov, N. Shcherban, O. Petrov, J. Lang, M. Shamzhy, M. Opanasenko and J. Čejka, *Inorg. Chem. Front.*, 2022, **9**, 1244–1257.
34 C. Wang, F. Jin, C. Ji and G. Wu, *Microporous Mesoporous Mater.*, 2021, **327**, 111440.
35 G. Lee, T. J. Sim, Y. Jeong, T. Lee, H. Baik, J. C. Jung, K.-S. Ha, S.-J. Cho, A. C. K. Yip and J. Choi, *Appl. Catal., A*, 2023, **659**, 119184.
36 Y. Zhang, M. Kubů, M. Mazur and J. Čejka, *Catal. Today*, 2019, **324**, 135–143.
37 L. Xu and J. Sun, *Adv. Energy Mater.*, 2016, **6**, 1600441.
38 Y. Zhou, Y. Mu, M.-F. Hsieh, B. Kabius, C. Pacheco, C. Bator, R. M. Rioux and J. D. Rimer, *J. Am. Chem. Soc.*, 2020, **142**, 8211–8222.
39 Z. Wang, M. O. Cichocka, Y. Luo, B. Zhang, H. Sun, Y. Tang and W. Yang, *Chin. J. Catal.*, 2020, **41**, 1062–1066.
40 M. Fabbiani, A. Morsli, G. Confalonieri, T. Cacciaguerra, F. Fajula, J. Haines, A. Bengueddach, R. Arletti and F. Di Renzo, *Microporous Mesoporous Mater.*, 2022, **332**, 111678.
41 L. L. Silva, M. J. Stellato, M. V. Rodrigues, B. J. Hare, J. C. Kenvin, A. S. Bommarius, L. Martins and C. Sievers, *J. Catal.*, 2022, **411**, 187–192.
42 S. L. Lawton, A. S. Fung, G. J. Kennedy, L. B. Alemany, C. D. Chang, G. H. Hatzikos, D. N. Lissy, M. K. Rubin, H.-K. C. Timken, S. Steuernagel and D. E. Woessner, *J. Phys. Chem.*, 1996, **100**, 3788–3798.
43 L. Xu, A. Martinez, S.-J. Hwang, K. Chaudhuri, S. I. Zones and A. Katz, *Inorg. Chem. Front.*, 2022, **9**, 4939–4951.
44 H. Li, C. Zhang, Q. Lin, F. Lin, T. Xiao, K. Yan, B. Shen, H. Zhang, Y. Tang and Z. Sun, *J. Am. Chem. Soc.*, 2024, **146**, 8520–8527.
45 J. Chen, Y. Li, Q. Hao, H. Chen, Z. Liu, C. Dai, J. Zhang, X. Ma and Z. Liu, *Natl. Sci. Rev.*, 2020, **8**, nwaa236.
46 W. J. Roth, *Studies in Surface Science and Catalysis*, Elsevier, 2005, vol. 158, pp. 19–26.

47 A. Korzeniowska, J. Grzybek, K. Kałahurska, M. Kubu, W. J. Roth and B. Gil, *Catal. Today*, 2020, **345**, 116–124.

48 W. J. Roth, D. L. Dorset and G. J. Kennedy, *Microporous Mesoporous Mater.*, 2011, **142**, 168–177.

49 A. Corma, M. J. Díaz-Cabanas, M. Moliner and C. Martínez, *J. Catal.*, 2006, **241**, 312–318.

50 L. Jiang, X. Li, Y. Gong, X. Meng, L. Zhang, Y. Zhai, S. Shang and L. Meng, *Microporous Mesoporous Mater.*, 2020, **302**, 110245.

51 S. Cao, P. Xiao, Q. Liu, Y. Ge, Z. Chen, Z. Li, Y. Gong, X. Yan and Z. Li, *Microporous Mesoporous Mater.*, 2024, **371**, 113088.

52 S. Cao, Y. Sun, Y. Shang, J. Wang, Y. Gong, G. Mo, Z. Li, Z. D. Zhang and A. Ma, *Mol. Catal.*, 2022, **524**, 112333.

53 S. Wang, Y. He, W. Jiao, J. Wang and W. Fan, *Curr. Opin. Chem. Eng.*, 2019, **23**, 146–154.

54 J. Bae and M. Dusselier, *Chem. Commun.*, 2023, **59**, 852–867.

55 K. Liu, S. Xie, S. Liu, G. Xu, N. Gao and L. Xu, *J. Catal.*, 2011, **283**, 68–74.

56 Y. Ding, Y. Zhao, D. Miao, Z. Wang, J. Feng, F. Jiao, X. Pan and X. Bao, *J. Phys. Chem. C*, 2024, **128**, 4508–4515.

57 Y. Ding, D. Miao, Z. Wang, J. Feng, P. Zhang, R. Yu, X. Cao, X. Pan and X. Bao, *ACS Catal.*, 2023, **13**, 14277–14284.

58 L. Liang, Y. Ji, Z. Zhao, C. M. Quinn, X. Han, X. Bao, T. Polenova and G. Hou, *Chem. Sci.*, 2021, **12**, 11554–11564.

59 X. Wang, W. Dai, G. Wu, L. Li, N. Guan and M. Hunger, *Microporous Mesoporous Mater.*, 2012, **151**, 99–106.

60 C. A. Emeis, *J. Catal.*, 1993, **141**, 347–354.

61 J. Dedecek, D. Kaucky, B. Wichterlova and O. Gonsiorova, *Phys. Chem. Chem. Phys.*, 2002, **4**, 5406–5413.

62 A. Palcic and V. Valtchev, *Appl. Catal., A*, 2020, **606**, 117795.

63 L. Tian, J. Li, Y. Li and B. Chen, *Chin. J. Catal.*, 2008, **29**, 889–894.

64 J. Chen, T. Liang, J. Li, S. Wang, Z. Qin, P. Wang, L. Huang, W. Fan and J. Wang, *ACS Catal.*, 2016, **6**, 2299–2313.

65 T. Liang, J. Chen, S. Wang, P. Wang, Z. Qin, F. Jin, M. Dong, J. Wang and W. Fan, *Catal. Sci. Technol.*, 2022, **12**, 6268–6284.

66 Y. Wang, S. Xu, X. He, F. Yang and X. Zhu, *Microporous Mesoporous Mater.*, 2022, **332**, 111677.

67 R. M. Mihályi, M. Kollár, P. Király, Z. Karoly and V. Mavrodinova, *Appl. Catal., A*, 2012, **417–418**, 76–86.

68 H. Wei, S. Xie, N. Gao, K. Liu, X. Liu, W. Xin, X. Li, S. Liu and L. Xu, *Appl. Catal., A*, 2015, **495**, 152–161.

69 E. M. Gallego, C. Paris, C. Martínez, M. Moliner and A. Corma, *Chem. Commun.*, 2018, **54**, 9989–9992.

70 Z. Wang, W. Chu, Z. Zhao, Z. Liu, H. Chen, D. Xiao, K. Gong, F. Li, X. Li and G. Hou, *J. Phys. Chem. Lett.*, 2021, **12**, 9398–9406.

71 Y. A. Wang, Y. Gao, S. J. Xie, S. L. Liu, F. C. Chen, W. J. Xin, X. X. Zhu, X. J. Li, N. Jiang and L. Y. Xu, *Catal. Today*, 2018, **316**, 71–77.

72 N. Gao, S. Xie, S. Liu, X. Li and L. Xu, *J. Porous Mater.*, 2013, **20**, 1217–1224.

73 W. J. Roth, C. T. Kresge, J. C. Vartuli, M. E. Leonowicz, A. S. Fung and S. B. Mccullen, *Stud. Surf. Sci. Catal.*, 1995, **94**, 301–308.

74 K. Ogorzały, G. Jajko, K. Wolski, S. Zapotoczny, M. Kubů, W. J. Roth, B. Gil and W. Makowski, *Catal. Today*, 2022, **390–391**, 272–280.

75 T. Wang, F. Jin, X. Yi, G. Wu and A. Zheng, *Microporous Mesoporous Mater.*, 2021, **310**, 110645.

76 L. Xu, T. Ma, Y. Shen, Y. Wang, L. Han, W. Chaittisilp, T. Yokoi, J. Sun, T. Wakihara and T. Okubo, *Angew. Chem., Int. Ed.*, 2020, **59**, 1–7.

77 F. Gong, N. Liu, L. Shi and X. Meng, *Fuel*, 2023, **344**, 128104.

78 K. Liu, S. Xie, H. Wei, X. Li, S. Liu and L. Xu, *Appl. Catal., A*, 2013, **468**, 288–295.

79 N. Gao, S. Xie, S. Liu, W. Xin, Y. Gao, X. Li, H. Wei, H. Liu and L. Xu, *Microporous Mesoporous Mater.*, 2015, **212**, 1–7.

80 H. Wei, S. Xie, N. Gao, K. Liu, X. Liu, W. Xin, X. Li, S. Liu and L. Xu, *Appl. Catal., A*, 2015, **495**, 152–161.

81 N. Gao, S. Xie, S. Liu, J. An, X. Zhu, L. Hu, H. Wei, X. Li and L. Xu, *Catal. Lett.*, 2014, **144**, 1296–1304.

82 C. Zhang, F. Lin, L. Kong, Z. Ye, D. Pan, H. Li, H. Li, P. Liu, Y. Zhang, H. Zhang and Y. Tang, *Inorg. Chem. Front.*, 2022, **9**, 4030–4040.

83 M. V. Rodrigues, C. Okolie, C. Sievers and L. Martins, *Cryst. Growth Des.*, 2019, **19**, 231–241.

84 W. J. Roth, M. Opanasenko, M. Mazur, B. Gil, J. Čejka and T. Sasaki, *Adv. Mater.*, 2024, **36**, 2307341.

85 A. V. Shkuropatov, A. G. Popov and I. I. Ivanova, *Pet. Chem.*, 2021, **61**, 908–915.

86 J. N. Armor, *Appl. Catal., A*, 2001, **222**, 407–426.

87 W. M. Yang, Z. D. Wang, H. M. Sun and B. Zhang, *Chin. J. Catal.*, 2016, **37**, 16–26.

88 B. Zhang, Z. Wang, P. Ji, Y. Liu, H. Sun, W. Yang and P. Wu, *Microporous Mesoporous Mater.*, 2013, **179**, 63–68.

89 W. Chu, S. Liu, W. Xin, Y. Wang, Z. Liu, C. Yang, Y. Wang, L. Xu, X. Li and X. Zhu, *Ind. Eng. Chem. Res.*, 2022, **61**, 2693–2700.

90 B. Liang, M.-N. Liu, N. An, F. Ren, Q.-X. Luo, H. Chen, J. Hu, X. Ma and Q.-Q. Hao, *Chem. Eng. J.*, 2024, **489**, 151109.

91 B. Liu, Z. Liao, Y. Wu, C. Ding, F. S. Butt, Y. Huang and J. Dong, *Mol. Catal.*, 2022, **531**, 112642.

92 R. Bao, Z. Shen, C. Ma, L. Li, Y. Wang, H. Sun and W. Yang, *Appl. Catal., A*, 2022, **643**, 118741.

93 V. P. S. Caldeira, A. G. D. Santos, D. S. Oliveira, R. B. Lima, L. D. Souza and S. B. C. Pergher, *J. Therm. Anal. Calorim.*, 2017, 1–13.

94 A. Corma, M. Davis, V. Fornés, V. González-Alfaro, R. Lobo and A. V. Orchillés, *J. Catal.*, 1997, **167**, 438–446.

95 G. Ma, Z. Liu, J. Fu and M. He, *Pet. Process. Petrochem.*, 2005, **36**, 11–15.

96 X. Ma, D. Zhou, X. Chu, D. Li, J. Wang, W. Song and Q. Xia, *Microporous Mesoporous Mater.*, 2017, **237**, 180–188.

97 P. Wu, T. Komatsu and T. Yashima, *Microporous Mesoporous Mater.*, 1998, **22**, 343–356.

98 V. Mavrodinova and M. Popova, *Catal. Commun.*, 2005, **6**, 247–252.

99 X. Ren, J. Liang and J. Wang, *J. Porous Mater.*, 2006, **13**, 353–357.

100 L. Su, Y. Li, W. Shen, Y. Xu and X. Bao, *Stud. Surf. Sci. Catal.*, 2004, **147**, 595–600.

101 J. Yang, J. Chu, J. Wang, D. Yin, J. Lu and Y. Zhang, *Chin. J. Catal.*, 2014, **35**, 49–57.

102 W. Lee, T. Lee, H.-G. Jang, S. J. Cho, J. Choi and K.-S. Ha, *Catal. Today*, 2018, **303**, 177–184.

103 P. Matias, J. M. Lopes, S. Laforge, P. Magnoux, M. Guisnet and F. R. Ribeiro, *Appl. Catal., A*, 2008, **351**, 174–183.

104 A. Peng, Y. Xing, G. Wu, X. Yu, X. Yi, X. Yan Liu, A. Zheng and F. Jin, *Chem. Eng. J.*, 2024, **485**, 150010.

105 T. Wan, F. Jin, X. Cheng, J. Gong, C. Wang, G. Wu and A. Liu, *Appl. Catal., A*, 2022, **637**, 118542.

106 A. Abutalib, D. Parmar, J. Kim and J. D. Rimer, *J. Catal.*, 2024, **433**, 115466.

107 S. Kweon, S. Oh, S. Lee, H.-K. Min and M. B. Park, *Chem. Eng. J.*, 2023, **476**, 146598.

108 W. Xu, X. Wang, W. Hou, K. Tang, X. Lu, Y. Gao, R. Ma, Y. Fu and W. Zhu, *J. Catal.*, 2022, **413**, 554–564.

109 T. Wang, W. Huang, H. Han, J. Zhang, H. Wu, X. Yan, Y. Jiang, L. Fang, B. Zhang, X. Guo and L. Ren, *Inorg. Chem. Front.*, 2022, **9**, 3505–3513.

110 C. H. L. Tempelman, R. Oozeerally and V. Degirmenci, *Catalysts*, 2021, **11**, 861.

111 I. Mongkolpichayarak, D. Jiraroj, W. Anutrasakda, C. Ngamcharussrivichai, J. S. M. Samec and D. Nuntasri Tungasmita, *J. Catal.*, 2021, **405**, 373–384.

112 H.-K. Min, S. Kweon, S. Oh, H. An, Y. Cho, H. Min, D. Jo, J. F. Kim, C.-H. Shin, S. B. Kang and M. B. Park, *Green Chem.*, 2021, **23**, 9489–9501.

113 X. Li, X. Yuan, G. Xia, J. Liang, C. Liu, Z. Wang and W. Yang, *J. Catal.*, 2020, **392**, 175–185.

114 W. Zhang, Y. Zhou, M. Shamzhy, S. Molitorisová, M. Opanasenko and A. Giroir-Fendler, *ACS Appl. Mater. Interfaces*, 2021, **13**, 15143–15158.

115 A. J. Schwanke, R. Balzer, C. W. Lopes, D. M. Meira, U. Díaz, S. Pergher and K. Bernardo-Gusmão, *Microporous Mesoporous Mater.*, 2021, **327**, 111425.

116 A. J. Schwanke, R. Balzer, C. W. Lopes, D. M. Meira, U. Diaz, A. Corma and S. Pergher, *Chem. – Eur. J.*, 2020, **26**, 10459–10470.

117 J. L. Chen, G. Peng, T. Y. Liang, W. B. Zhang, W. Zheng, H. R. Zhao, L. Guo and X. Q. Wu, *Nanomaterials*, 2020, **10**, 20.

118 X. Meng, F. Jin, A. Qiang Peng, X. Jiang, X. Guo and G. Wu, *Fuel*, 2024, **363**, 130968.

119 S. Liu, G. Wu, J. Gong, J. Wang, X. Meng, X. Guo and F. Jin, *Chem. Eng. J.*, 2023, **476**, 146410.

120 K. Kałahurska, W. Pajerski, A. Kotarba, M. Kubů, Y. Zhang, M. Mazur, J. Přech, G. Jajko, W. Makowski, W. J. Roth and B. Gil, *Catal. Today*, 2022, **390–391**, 335–342.

121 N. P. Nimisha, S. B. Narendranath and A. Sakthivel, *Chem. Commun.*, 2024, **60**, 1480–1483.

122 E.-J. Kim, Y. Woo Kim, Y. Cho, S. Kweon, M. Bum Park, C.-H. Shin, H.-K. Min and K. An, *Chem. Eng. J.*, 2024, **485**, 149871.

123 L. Liu, U. Díaz, R. Arenal, G. Agostini, P. Concepción and A. Corma, *Nat. Mater.*, 2017, **16**, 132–138.

124 L. C. Liu, D. N. Zakharov, R. Arenal, P. Concepcion, E. A. Stach and A. Corma, *Nat. Commun.*, 2018, **9**, 10.

125 P. He, Q. Yi, H. Geng, Y. Shao, M. Liu, Z. Wu, W. Luo, Y. Liu and V. Valtchev, *ACS Catal.*, 2022, **12**, 14717–14726.

126 S. Kweon, Y. W. Kim, J. Bae, E.-J. Kim, M. B. Park and H.-K. Min, *J. CO2 Util.*, 2022, **58**, 101921.

127 L. K. Zhang, X. Y. Chen, Y. Ma, S. J. Song, H. Xu, Y. J. Guan, W. Y. Song, J. W. Zhang and P. Wu, *ACS Catal.*, 2024, **14**, 9431–9439.

128 R. Roque-Malherbe, R. Wendelbo, A. Mifsud and A. Corma, *J. Phys. Chem.*, 1996, **27**, 14064–14071.

129 F. Zhao, X. S. Sun, R. F. Lu and L. H. Kang, *Can. J. Chem.*, 2017, **95**, 1241–1247.

130 A. Zukal and M. Kubu, *Dalton Trans.*, 2014, **43**, 10558–10565.

131 J. Pawlesa, A. Zukal and J. Čejka, *Adsorption*, 2007, **13**, 257–265.

132 A. Zukal, M. Kubů and J. Pastva, *J. CO2 Util.*, 2017, **21**, 9–16.

133 S. Wang, H. Li, S. Xie, S. Liu and L. Xu, *Chemosphere*, 2006, **65**, 82–87.

134 S. Wang, H. Li and L. Xu, *J. Colloid Interface Sci.*, 2006, **295**, 71–78.

135 T. Terdkiatburana, S. Wang and M. O. Tadé, *Chem. Eng. J.*, 2008, **139**, 437–444.

136 C. Wang, N. Sakai, Y. Ebina, T. Kikuchi, J. Grzybek, W. J. Roth, B. Gil, R. Ma and T. Sasaki, *Small*, 2024, **20**, 2308293.

137 C. Zhang, Y. Huang, H. Zhao, H. Zhang, Z. Ye, P. Liu, Y. Zhang and Y. Tang, *ACS Appl. Nano Mater.*, 2021, **4**, 10645–10656.

138 Z. Zeng, F. Ma, S. Wang, J. Wen, X. Jiang, G. Li, Y. Tong, X. Liu and J. Jiang, *J. Am. Chem. Soc.*, 2024, **146**, 9851–9859.

139 X. Ji, Y. Bao, C. Du, Q. Shi, W. Xu and Z. Wang, *Desalination*, 2022, **541**, 116023.